Current Research in Chemical Biology 2 (2022) 100022

Contents lists available at ScienceDirect

Current Research in Chemical Biology

journal homepage: www.journals.elsevier.com/current-research-in-chemical-biology

The druggability of the ATP binding site of glycogen phosphorylase kinase probed by coumarin analogues

Serafeim Alexopoulos [a], Anastasia Gkouskou [a], George Stravodimos [a], Anastasia S. Tsagkarakou [a], Ioannis Tsialtas [a], Demetres Katounis [a], Anna-Maria G. Psarra [a], Demetres Leonidas [a], Goutam Brahmachari [b], Joseph M. Hayes [c], Vasiliki Skamnaki [a,*]

[a] Department of Biochemistry and Biotechnology, University of Thessaly, Biopolis 41500, Larisa, Greece
[b] Laboratory of Natural Products & Organic Synthesis, Department of Chemistry, Visva-Bharati (a Central University), Santiniketan-731 235, West Bengal, India
[c] School of Pharmacy and Biomedical Sciences University of Central Lancashire, Preston PR12HE, UK

ARTICLE INFO

Keywords:
Kinase inhibitors
Coumarin analogues
Drug design
Glycogen phosphorylase kinase
Diabetes

ABSTRACT

Glycogen phosphorylase kinase (PhK) converts by phosphorylation, the inactive glycogen phosphorylase (GPb) into active GPa in the glycogenolytic pathway. It is a complex enzyme comprising of the catalytic (γ) and three regulatory subunits (α, β, δ) forming a hexadecamer with stoichiometry $(\alpha\beta\gamma\delta)_4$. Several studies have indicated PhK as a promising target for the development of antihyperglycemics as its inhibition blocks glycogenolysis in liver and a potential therapeutic target for cancer against pathological angiogenesis and tumor progression. The identification of compounds that inhibit the kinase through their direct binding to its catalytic site is an effective approach to identify bioactive molecules of therapeutic significance. Towards this, the structure of the N-terminal kinase domain (residues 1–298) of the catalytic γ subunit of PhK (PhKγtrnc) has been determined by X-ray crystallography while staurosporine and indirubin analogues have been characterized as potent inhibitors targeting the ATP binding site. In this study, a series of 38 synthetic analogues of naturally occurring coumarins were screened for inhibition of PhKγtrnc, *in vitro*, using a photometric assay. The IC_{50} values of the two most potent compounds were determined for PhKγtrnc and the pharmacologically relevant target, human liver isoform (PHKG2A). Their cellular efficacy and toxicity in HepG2 cells were further assessed *ex vivo*. Docking experiments and the structural comparison with previously described inhibitors reveal the binding mode of the coumarin scaffold at a no hinge region of the ATP site of PhK and the role of a conserved β3-Lys in binding. The experimental findings provide structural insights with implications to the kinase targeting and drug design.

1. Introduction

Glycogen phosphorylase kinase (PhK) plays a key role in glycogen metabolism. It catalyzes the Ca^{2+} dependent phosphorylation of glycogen phosphorylase (GP), converting inactive GPb into active GPa promoting thus, glycogenolysis (Fig. 1).

Studies on cellular and animal models have shown that inhibition of liver PhK selectively blocks glycogenolysis (Begum et al., 2015; Aiston et al., 2003), indicating it as a target for the development of anti-hyperglycaemic agents. Moreover, it has been shown (Camus et al., 2012) that there is a link between upregulated PhK gene expression and tumorigenesis connecting glycogen metabolism with pathological angiogenesis and tumor progression, identifying thus, PhK also as a novel therapeutic target for cancer. PhK is one of the most complex protein kinases in nature, composed of four types of subunits, with stoichiometry $(\alpha\beta\gamma\delta)_4$ resulting in a molecular mass of 1.3×10^6 Da. The α and β are the regulatory subunits and are targets of control through phosphorylation by PKA while the δ subunit is calmodulin and confers calcium sensitivity. The catalytic γ subunit has 386 residues and is comprised of an N-terminal kinase domain (residues 1–298) and a calmodulin binding domain (residues 299–386). The kinase domain comprises of the structural elements required to achieve catalysis and is constitutively active.

The structures of the kinase domain (residues 1–298) of the γ subunit of rabbit muscle PhK (PhKγtrnc) in complex with nucleotides (ATP and AMPPMP) and a peptide substrate have been determined and a catalytic mechanism has been proposed (Lowe et al., 1997; Skamnaki and Oikonomakos, 2000; Skamnaki et al., 1999). Notably, PhKγtrnc has 94% sequence identity with the human muscle isoform. In addition, the crystal

* Corresponding author.
E-mail address: vskamnaki@bio.uth.gr (V. Skamnaki).

https://doi.org/10.1016/j.crchbi.2022.100022

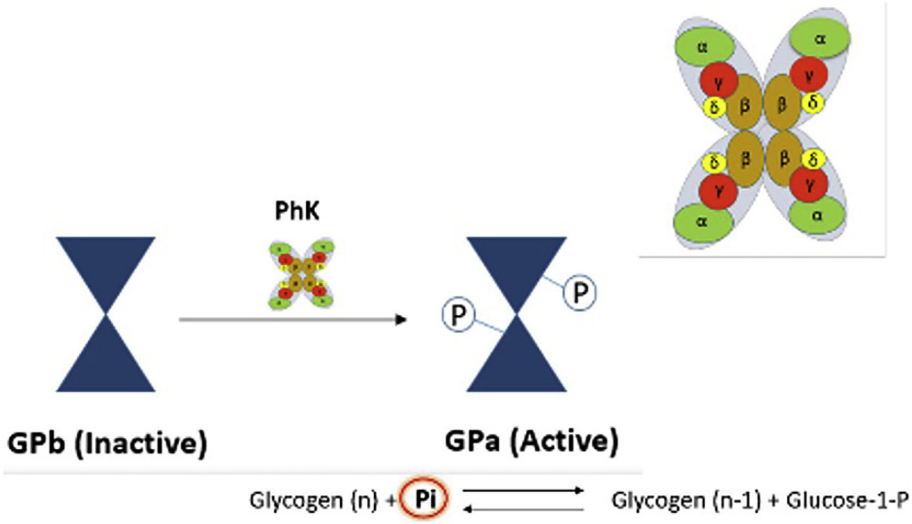

Fig. 1. Schematic diagram of the reaction catalyzed by PhK. Upon activation by hormonal or neuronal signals, PhK catalyzes the conversion of inactive GPb to active GPa. GPa in turn catalyzes the first step in glycogenolysis. Inset: Representation of the hexadecamer of the PhK holoenzyme.

structure of the kinase domain (residues 6–293) of human liver PhK (PHKG2A) in complex with sunitinib (PDB: 2Y7J) has been solved. The overall highly conserved kinase fold comprises of the N-terminal lobe (residues 18–105 in PhKγtnc, and 22–109 in PHKG2A) which is composed by five strands of antiparallel β sheets (β1–β5) and one α-helix, the aC helix. The C-terminal lobe (residues 110–292 in PhKγtrnc, and 114–296 in PHKG2A) is comprised mostly by α-helices and is connected to the N-terminal lobe by a hinge region (residues 105–110 in PhKγtrnc and 109–114 in PHKG2A). The ATP binding site is situated at the interface of the two lobes. Secondary structural elements of a kinase domain including the glycine loop for localization of phosphates of ATP, the catalytic Asp149 (Asp153 in PHKG2A) and the bulky gatekeeper Phe103 (Phe 107 in PHKG2A) are also conserved between the two isoforms. Kinetic studies indicated staurosporine (K_i = 0.37 nM) and indirubin analogues as potent ATP competitive inhibitors while the most potent and selective inhibitor for rabbit muscle PhK identified to date is the staurosporine analogue KT5720 (K_i = 18.4 nM) (Begum et al., 2015; Hayes et al., 2011). The most potent indirubins had *IC*50 values of 0.17–0.36 μM. Indirubin-3-acetoxime was the most potent, with the 3′-acetoxime group more favorable for PhK inhibition compared to other kinases (Begum et al., 2015). These studies revealed that most inhibitors bind in the same active site area as the ATP adenine ring and, as in homologous kinase complexes, the platform for inhibitor binding is hydrogen bonding with hinge region residues. Despite this, structure based inhibitor design efforts targeting human liver PhK are to date limited. Targeting the highly conserved residues among kinases ATP binding sites imposes always a selectivity challenge for type I inhibitors. Different chemical scaffolds need to be explored for potency and selectivity against PhK exploiting enzyme's peculiarities in archetypal structural elements of the active site.

Coumarins comprise a broad class of 1,2 benzopyrone derivatives widely distributed in plants, fungi, and bacteria as secondary metabolism products with diverse pharmacological properties. They have also been used as antimicrobial, antibacterial, antifungal, antioxidant and antitumor agents (Pereira et al., 2018). The coumarin moiety (Table 1a.) can form a variety of noncovalent interactions including hydrogen bonds, electrostatic, π-π and hydrophobic interactions with different target proteins and enzymes including a number of protein kinases (Thakur et al., 2015; Katsori and Hadjipavlou-Litina, 2014). A variety of functional groups on the coumarin scaffold has been explored in targeting several kinases in numerous studies (Nasr et al., 2014; Kaur et al., 2015). In this work we assessed the inhibition potency of 38 functionalized coumarin analogues to the rabbit muscle kinase domain of the catalytic γ subunit (PhKγtrnc). The IC_{50} values of the two most potent inhibitors against PhKγtrnc and the pharmacologically relevant target human liver isoform (PHKG2A) were determined while their *ex vivo* antihyperglycaemic efficacy was assessed. Despite the moderate potency of the inhibitors *in vitro*, docking experiments suggest a potential different mode of binding dominated by the interaction of the coumarin scaffold with conserved β3-Lys away from the hinge region residues.

2. Materials and methods

2.1. Chemical synthesis

All the 38 functionalized 2-aryl-4-alkyl/aryl-pyrano [3,2-*c*]chromen-5(4*H*)-ones (GB-P2-4a-4z″) and 3-/4-(5-oxo-2-aryl-4,5-dihydropyrano [3,2-*c*]chromen-4-yl)benzaldehydes (GB-P2-4′a-4′j) (Table 1) were synthesized following a green method previously reported (Brahmachari and Nurjamal, 2017), based on a catalyst-free three-component reaction between alkyl/aryl aldehydes, acetophenones and 4-hydroxycoumarin in aqueous ethanol at ambient condition, and the synthesized and purified products were fully-characterized by their analytical as well as detailed spectral studies including FT-IR, NMR and mass.

2.2. Protein production and purification

Rabbit muscle PhKγtrnc was expressed as an N-terminal glutathione-S-transferase (GST) fusion as described previously (Hayes et al., 2011). The PHKG2 gene encoding the kinase domain (PHKG2A) of the human liver γ subunit of PhK (residues 1–300) was synthesized after codon usage optimization, cloned into the plasmid vector pET-42a (+), and then transformed into *E. coli* BL21Gold (DE3) competent cells. After optimization of expression conditions, protein overexpression was achieved by induction with 0.5 mM IPTG and incubation (with shaking) at 18 °C for 16 h. The protein was expressed soluble in high yield and was purified by an affinity chromatography (GST Trap) step followed by precision protease digestion. A cibacron blue (Sigma) affinity chromatography column was used as a second step in protein purification followed by a (GST Trap) cleaning up final step. Rabbit muscle glycogen phosphorylase b (GPb) was purified as previously described (Drakou et al., 2020). Its concentration was determined from absorbance measurements at 280 nm using an absorbance index A1% = 13.2.

Table 1
Chemical structures and percentages of inhibition of PhKγtrnc at 50μM of 2-aryl-4-alkyl/aryl-pyrano (Camus et al., 2012) chromen-5(4H)-ones (GB-P2-4a-4z″) and 3-/4-(5-oxo-2-aryl-4,5-dihydropyrano (Camus et al., 2012) chromen-4-yl)benzaldehydes (GB-P2-4′a-4′j).

a 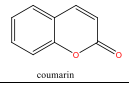 coumarin 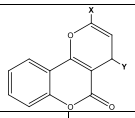				% inhibition
	Compound name	X	Y	
1	GB-P2-4a		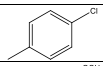	33%
2	GB-P2-4b		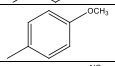	17%
3	GB-P2 -4c		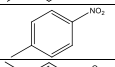	6%
4	GB-P2-4d		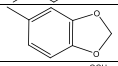	4%
5	GB-P2-4e	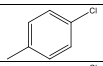	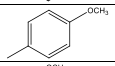	8%
6	GB-P2-4f	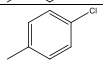	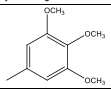	7%
7	GB-P2-4g	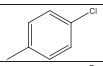	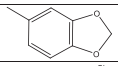	10%
8	GB-P2-4h	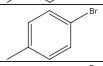	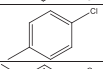	12%
9	GB-P2-4i	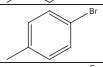	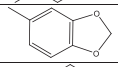	8%
10	GB-P2-4j	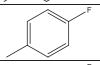		18%
11	GB-P2-4k	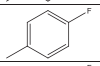	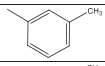	7%
12	GB-P2-4l	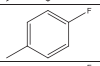	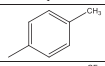	2%
13	GB-P2-4m	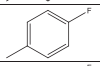	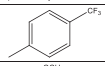	13%
14	GB-P2-4n	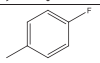	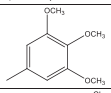	4%
15	GB-P2-4o	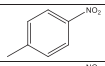	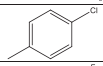	17%
16	GB-P2-4p	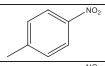	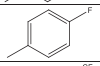	3%
17	GB-P2-4q	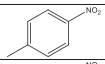	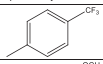	16%
18	GB-P2-4r	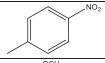	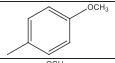	15%
19	GB-P2-4s	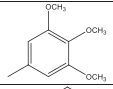	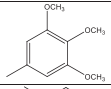	4%
20	GB-P2-4t			18%
21	GB-P2-4u	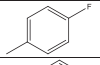		13%
22	GB-P2-4v			9%
23	GB-P2-4w		$CH_2CH_2CH_3$	9%
24	GB-P2-4x	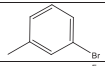	$CH_2CH_2CH_3$	16%
25	GB-P2-4y	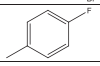	$CH_2CH_2CH_3$	6%

26	GB-P2 -4z			1%
27	GB-P2-4z′	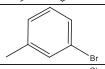		5%
28	GB-P2-4z′′	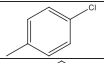		5%
29	GB-P2-4′a			32%
30	GB-P2-4′b	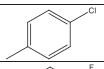		12%
31	GB-P2-4′c	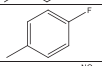		16%
32	GB-P2-4′d	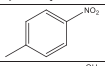		10%
33	GB-P2-4′e	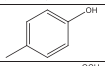		13%
34	GB-P2-4′f	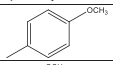		12%
35	GB-P2-4′g	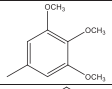		12%
36	GB-P2-4′h			16%
37	GB-P2-4′i			28.5%
38	GB-P2-4′j	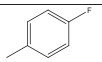		30%

2.3. Kinetic screening and IC50 determination

All compounds (Table 1) were screened against PhKγtrnc by measuring percentage of inhibition at a single concentration of 50 μM, in the presence of 0.1 mM ATP and 10 μM GPb. The concentration of PhKγtrnc was 30 nM. A two-stage kinetic assay was used to evaluate the potency of the inhibitors where the enzymatic activities of PhK (PhKγtrnc and PHKG2A) were measured by monitoring the conversion of GPb to GPa by assaying phosphorylase activity in the presence of 10 μM AMP and 0.5 mM caffeine in the direction of glycogen synthesis (Hayes et al., 2011; Drakou et al., 2020). For the IC_{50} determination the activities were assayed at constant concentrations of GPb (1 mg/mL) and ATP (0.1 mM). Blank values were subtracted, and activities were calculated after 12 min of incubation at 30 °C. The concentration of the various coumarin analogues tested varied from 30 μM to 350 μM during the assay. In the experiments with the human liver isoform, the concentration of PHKG2 was 10 ng/mL in the assay conditions. Activities were expressed as percentages of the maximal activity (i.e., in the absence of inhibitors). Most of the inhibitors showed adequate solubility up to 1% (v/v) in DMSO and the presence of the solvent did not affect the activities of both enzyme forms if the final concentration in the assay was kept below 5% (v/v). Apart from GB-P2-4′j none of the other compounds tested showed significant inhibition towards GPb. Data was analyzed using the non-linear regression program GraFit (Leatherbarrow, 2007).

2.4. Ex vivo assays

HepG2 cells were maintained and seeded at a density 1.75×10^6 cells per dish using Dulbecco's modified Eagle's medium (DMEM) supplemented with 25 mM glucose, 10% fetal bovine serum (FBS), 2 mM L-glutamine, and penicillin/streptomycin and cultured at 37 °C in a 5% CO_2 incubator. After 16–18 h the glycogen synthesis was induced by high-glucose DMEM medium without L-glutamine and FBS in the presence of penicillin/streptomycin, 10 nM dexamethasone, and 100 nM insulin. Following overnight incubation the cells were incubated for 3 h in the absence or presence of different concentrations (200 μM and 400 μM) of GB-P2-4A or GB-P2-4′A in a DMEM medium without phenol red, L-glutamine, FBS, and glucose in addition of 100 nM glucagon for induction of glycogenolysis. Cells were then washed with DMEM and harvested by centrifugation at 380 rcf and 4 °C for 5 min. The cells were lysed in a buffer containing 20 mM HEPES/NaOH, pH 7, 1 mM NaF, 1 mM PMSF, and 0.05% w/v Triton and sonicated on ice four times for 1 s. The cell lysates were centrifuged at 15,600 rcf and 4 °C for 15 min and the total protein concentration in the supernatants determined by the Bradford method (Bradford, 1976). GPa activity was measured in the direction of glycogen synthesis by monitoring the release of inorganic phosphate. The cell lysates were mixed with 1% w/v glycogen and pre-incubated for 15 min at 30 °C, before initiating the reaction with 30 mM Glc-1P as described (Drakou et al., 2020). For the calculation and statistical evaluation of kinetic data, the nonlinear regression program GraFit (Leatherbarrow, 2007) was used. Cell cytotoxicity of the inhibitors was evaluated using the 3-[4,5-dimethylthiazole-2-yl]-2,5-diphenyltetrazolium bromide (MTT) assay (Mosmann, 1983).

2.5. In silico studies

2.5.1. Protein preparation

The initial setup of the PhK protein for calculations was performed using Protein Preparations Wizard (Schrodinger, 2018) using solved co-crystallized complex structures for both rabbit muscle (PDB code: 1PHK, 2.20 Å resolution) and human liver (PDB code: 2Y7J, 2.50 Å resolution). Bond orders were assigned and hydrogen atoms added, with protonation states for basic/acidic residues based on calculated residue *pKa* values from PROPKA (Sondergaard et al., 2011) at normal pH (7.0).

Subsequent optimization of hydroxyl groups, histidine protonation states and C/N atom "flips", and side-chain O/N atom flips of Asn and Gln residues was based on optimizing hydrogen bonding patterns. Water molecules within 5 Å of HET groups were initially retained but deleted for subsequent docking. Finally, Impref minimizations of the PhK complexes were performed using the OPLSe forcefield (Harder et al., 2016) to remove any steric clashes and bad contacts, but with the RMSD of all heavy atoms was within 0.3 Å of the crystallographic positions. 2Y7J consisted of four chains A-D but only chain A was considered in docking calculations.

2.5.2. Ligand preparation

The GB-P2-4a and GB-P2-4′a ligands were prepared for docking calculations using LigPrep (Schrodinger, 2018) and OPLSe at a pH of 7.0 ± 2.0, generating as expected only neutral states of ligands.

2.5.3. Docking details

Docking calculations were performed using Glide v8.1 (Schrodinger LLC, New York, NY, 2018) to rabbit muscle and human liver PhK structures, the preparation of which is described above. The shape and properties of the PhK ATP-binding sites were first mapped onto grids with dimensions of ~27 × 27 × 27 Å centered on the respective native cocrystallized ligand. Standard parameters were applied including default OPLSe atomic charges and van der Waals scaling (0.8) for ligand nonpolar atoms to include modest 'induced fit' effects. Docking calculations were performed in Glide-SP mode including post-docking minimization with strain correction. The top-ranked binding pose (GlideScore) for each ligand was considered for further analysis. The programs CONTACT as implemented in CCP4 suite (Winn et al., 2011) and PLIP (Adasme et al., 2021) were used for analysis of protein-ligand interactions and the figures were created using PYMOL (DeLano, 2002) and LigPlot (Wallace et al., 1995).

3. Results and discussion

3.1. Inhibition studies

The percentage of inhibition at 50 μM of all 38 coumarin analogues against PhKγtrnc is shown in Table 1. The most potent compounds of initial screening were GB-P2-4a, GB-P2-4j, GB-P2-4°, GB-P2-4′a, GB-P2-4′i και GB-P2-4′j. Compounds GB-P2-4a, GB-P2-4′a, GB-P2-4j, presented over 30% inhibition and their IC_{50} values against rabbit muscle PhKγtrnc and human liver PHKG2A were determined (Table 2). GB-P2-4′j exhibited strong inhibition against GP and was excluded. The inhibition of GB-P2-4a (4-(4-Chlorophenyl)-2-phenylpyrano chromen-5(4H)-one) and GB-P2-4′a (-(5-Oxo-2-phenyl-4,5-dihydropyrano chromen-4-yl)benzaldehyde) against GP was negligible and were further studied as hit compounds. The IC_{50} values of GB-P2-4a were 95 ± 1.4 μM and 61.5 ± 0.47 μM for PhKγtrnc and PHKG2A, respectively. Accordingly, the IC_{50} values of GB-P2-4′a were measured 102.6 ± 1.7 μM against PhKγtrnc and 50.5 ± 0.35 μM against PHKG2A. Both compounds showed *in vitro,* increased potency (2x) for the human liver PhK isoform and this difference reflects additional polar contacts, although, decreased potency for both PhK isoforms compared to staurosporine (K_i's in nM range) or indirubin analogues (IC_{50} values 0.17–0.36 μM) (Begum et al., 2015; Hayes et al., 2011). The toxicity of both compounds towards hepatocarcinoma HepG2 cells was assessed as described in Experimental Section applying the MTT assay. No cytotoxicity was observed upon 3h incubation of the cells at inhibitor concentrations up to 400 μM (Fig. 2A) The efficacy of both compounds to inhibit glycogenolysis was further assessed through determination of the GPa activity in an *ex vivo* system of hepatocarcinoma HepG2 cells in culture. *In vitro* assay of human liver GPa showed no inhibition for both compounds at concentrations 400 μM. Hence any reduction in GPa activity, *ex vivo* in HepG2 cells, reflects decreased production of hepatic GPa through inhibition of upstream PhK. Treatment of HepG2 cells for 3 h with 200 μM and 400 μM of GB-P2-4a resulted in 14.2% and 25.3% inhibition of GPa, respectively. Accordingly, 3h treatment of HepG2 cells with 200 μM and 400 μM of GB-P2-4′a resulted in 6.7% and 8.9% GPa inhibition, respectively (Fig. 2B). GB-P2-4′a exhibits less cellular efficacy despite its higher potency *in vitro.* Both inhibitors, although not cytotoxic, show low but not negligible inhibition of PhK at cellular level which is in agreement with their moderate potency *in vitro* studies.

Table 2
IC50 values of GB-P2-4a and GB-P2-4′a.

Inhibitor		IC50 (μM)	
Name	Chemical Structure	PhKγtrnc	PHKG2A
GB-P2-4a	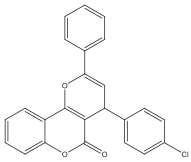	95 ± 1.4	61.5 ± 0.5
GB-P2-4′a	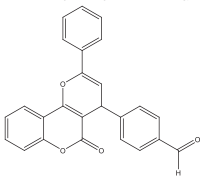	102.6 ± 1.7	50.5 ± 0.3

3.2. Ligand binding

Inspection of the protein-ligand docking poses showed that in both isoforms, GB-P2-4a and GB-P2-4′a bind at the ATP binding site as type I kinase inhibitors. The interactions of the ligands with protein residues are shown in Table 3. In the GB-P2-4a complexes, one oxygen (O15) of the coumarin moiety (chromen-2-one ring) is posed at a strong hydrogen bond forming distance of 3.1 Å from the (NZ) of the conserved Lys 48, for PhKγtrnc and 2.9 Å from Lys 53 (NZ) for PHKG2A (Fig. 3). A halogen bond is formed between the chlorine atom and Lys 151 (NZ) in PhKγtrnc and Lys 155 (NZ) in PHKG2A, respectively. In addition, 60 van der Waals interactions (22 polar/nonpolar, 37 nonpolar/nonpolar, 1 polar/polar) are formed with residues in the PhKγtrnc complex and 65 (6 polar/polar, 37 polar/nonpolar, 22 nonpolar/nonpolar) in PHKG2A respectively. Similar binding modes are shown in GB-P2-4′a complexes where the coumarin (O15) forms one hydrogen bond with Lys 48 in PhKγtrnc and 2 hydrogen bonds from atoms (O15) and (O21) with the NZ atom of Lys53 in PHKG2A (Fig. 3). In the case of GB-P2-4′a chlorine is replaced by a carbonyl group providing an extra oxygen (O29) that in PHKG2A complex forms a strong hydrogen bond with Lys 155 (NZ). GB-P2-4′a also forms 64 van der Waals interactions (2 polar/polar, 24 polar/nonpolar, 38 non polar/nonpolar) with PhKγtrnc and 63 van der Waals interactions (4 polar/polar, 36 polar/nonpolar, 23 nonpolar/nonpolar) with PHKG2A. These interactions are in good agreement with inhibitor IC_{50} values. Overall, both compounds form more polar interactions with the liver isoform with Asp171 participating in the majority of them, while the gatekeeper Phe107 (Phe103 in PhKγtrnc) contributes significantly (about 15%) to hydrophobic interactions. The gatekeeper residues in kinases guard the entrance of a hydrophobic pocket adjacent to the adenine binding pocket, the so-called 'p38' pocket (recognized in the p38α–BIRB-796 complex and in the Abl–imatinib complex) (Johnson, 2009a). The distribution of gatekeeper residues in kinome has been studied (Zuccotto et al., 2010; Vulpetti and Bosotti, 2004; Scapin et al., 2003) showing Met as the most frequent (40%) gatekeeper residue of the analyzed set, while the bulky aromatic Tyr or Phe residues have about 16% frequency. Given that, adding groups to the coumarin scaffold forming hydrophobic or strong π-stacking interactions with the gatekeeper Phe could provide further elements of potency and selectivity for future drug design. The planar nature in addition to

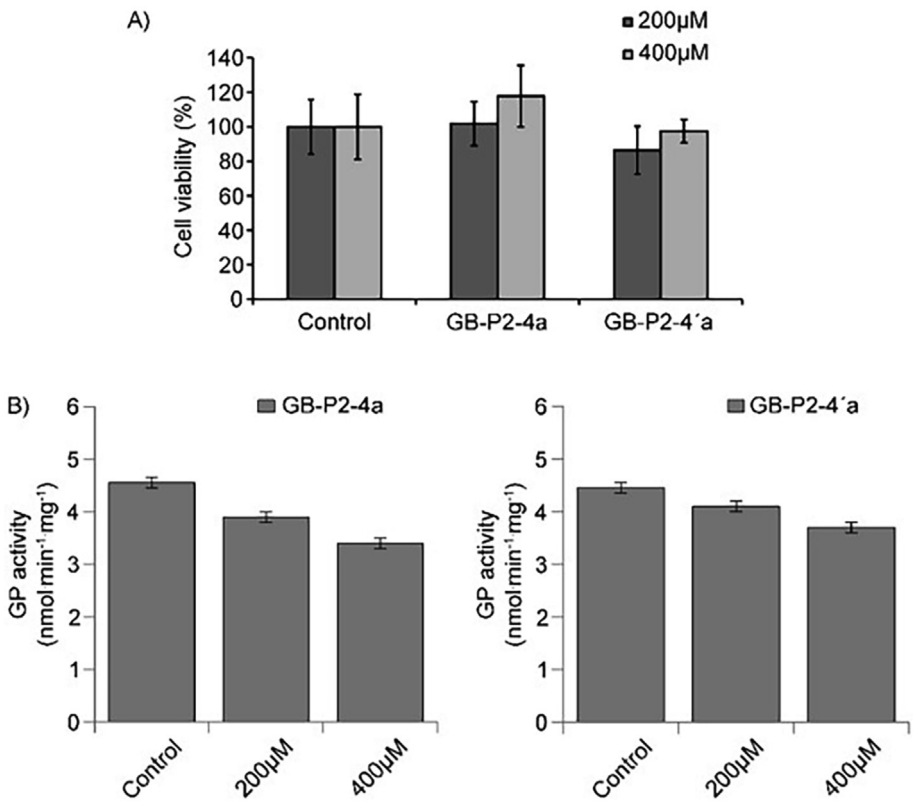

Fig. 2. A) The viability of HepG2 cells upon 3 h treatment with GB-P2-4a and GB-P2-4′a measured applying MTT assay. The vehicle treated, control, cells were set at 100%. Data were analyzed by one-way ANOVA followed by Tukeys's post hoc test and expressed as mean ± S.D. (n = 4). No statistical differences were observed. B) Effect of GB-P2-4a and GB-P2-4′a on the activity of GP in HepG2 cells.

structure complementarity with protein of both ligands favors binding at the ATP binding site although, their moderate potency can be attributed to the lack of groups participating in hydrogen bonds. In all cases, the ligand orientations are such that hydrogen bond interactions of the coumarin moiety with the conserved Lys53 (Lys48 in PhKγtrnc) are the structural determinants of potency. This lysine of the β3 strand contacts the oxygens of α and β phosphates helping in the localization of phosphates during ATP binding (Johnson et al., 1998). No other PhK ligands are reported to exploit interactions with this β3 lysine to date.

3.3. Structural comparison of isoforms

Alignment of the structures of the binary complex PhKγtrnc-ATP/Mg2+ (1phk, Chain A), with PHKG2A-sunitinib (2y7j, Chain A) using the pairwise structure alignment PDB tool showed overall 86% similarity (70% sequence identity) and overall RMSD 1.21 Å. Both structures adopt the conserved features of the kinase domain fold (Johnson et al., 1998). The activation segment (residues 167–191 in PhK) is defined as the region spanning the conserved sequences DFG (residues 167–169) and APE (residues 191–193) Fig. 4A. The activation segment is important for substrate recognition as well as overall catalytic efficiency. The central part of this segment shows little sequence conservation and yet plays a crucial role in the activation by phosphorylation of a Ser or Thr in different kinases. PhK is active without the requirement for phosphorylation as its Glu182 (Glu186 in PHKG2A) mimics the interactions of phosphorylated residue. In active kinases the DFG motif adopts the so called DFG-in conformation where the aspartate of the DFG points into the ATP site and binds the metal, the phenylalanine of the DFG is buried in a hydrophobic pocket and is not accessible. In the inactive conformation, the aspartate of the DFG motif points out so that it can no longer bind the coordinating magnesium ion and the phenylalanine is directed towards the ATP site (Johnson, 2009b). Actually, the structure of the PhKγtrnc-ATP/Mg2+ complex shows that the DGF motif adopts the DFG-in conformation of active kinases. Interestingly, superposition of the PhKγtrnc-ATP/Mg2+ with that PHKG2A-sunitinib show that the Asp171 in PHKG2A is shifted away the ATP binding site although Phe172 remains in same position seemingly adopting a DFG-out conformation (Fig. 4A). In the absence of the ATP/Mg2+ no interactions are formed by Asp171 stabilizing a DFG-in conformation. This shift to DFG-out conforming with inactive kinases is unlikely due to the presence of the inhibitor since sunitinib does not form any shift causing interactions. It can be rather attributed to the lack of metal. Most interestingly, in the case of PHKG2A-GB-P2-4a complex the Asp171 is posed in hydrogen bonding distance with the coumarin's O15. This interaction potentially stabilizes this DFG out conformation favoring thus, kinase inhibition. In case of the PHKG2A-GB-P2-4′a complex the interaction via a strong hydrogen bond of the inhibitor's carbonyl oxygen (O29) with Lys155 shifts the inhibitor away from Asp171 precluding hydrogen binding. In addition, Lys48 in PhKγtrnc is part of the K/E/D/D (Lys/Glu/Asp/Asp) signature motif that exists in nearly all active kinases (Roskoski, 2015) and forms a salt bridge with a conserved glutamate (Glu73) near the center of the αC-helix of the kinase domain. The inward conformation of this aC helix favors active state in contrast to aC outward conformation. In case of PHKG2A the corresponding Lys53 is poised away failing to form a strong interaction adopting an aC outward conformation (Fig. 4B). In PHKG2A inhibitor complexes the attraction of Lys53 via the hydrogen bond interactions towards coumarin moiety precludes it interactions with the Glu77 disfavoring aC inward conformation. The sunitinib complex provides a snapshot of the activation segment and the aC helix in a less active conformation. The binding of GB-P2-4a and GB-P2-4′a

Table 3
A) Hydrogen bond and B) van der Waals interactions of GB-P2-4a and GB-P2-4' a with PhK isoforms.

A. Hydrogen bond interactions

GB-P2-4a atom	PhKγtrnc atom	Distance (Å)	PHKG2A atom	Distance (Å)
O15	Lys48 (NZ)	3.07	Lys53 (NZ)	2.89
Cl (Halogen bond)	Lys151 (NZ)	3.45	Lys155 (NZ)	3.91
GB-P2-4′'a atom	**PhKγtrnc atom**	**Distance (Å)**	**PHKG2A atom**	**Distance (Å)**
O15	Lys48 (NZ)	3.07	Lys53 (NZ)	3.22
O21	–	–	Lys53 (NZ)	3.11
O29	–	–	Lys155	2.91

B. Van der Waals interactions

GB-P2-4a atom	PhKγtrnc atom	Number of contacts
C1	Leu156 CD1;	1
C2	Leu156 CD1; Leu25 CB;	2
C3	Met106 O; Leu156 CD1; Leu25 CB;	3
C4	Gly109 CA;	1
C5	Gly109 CA; Glu110 CG; Leu25 O;	3
C6	Glu110 CG; Leu25 O; Glu110 OE2;	3
C9	Val33 CG2;	1
C10	Gly26 CA;	1
C11	Val33 CG2;	1
C12	Val33 CG2;	1
C14	Asp167 N; Lys48 CD; Lys48 NZ;	3
O15	Asp167 CB; Lys48 CD; Lys48 CE;	3
C16	Lys48 CE; Lys48 NZ;	2
C17	Thr166 CB; Thr166 CG2;	2
O8	Leu156 CD1;	1
C18	Phe103 CG; Phe103 CD2; Thr166 CB; Thr166 CG2; Phe103 CE2;	5
C19	Phe103 CD2; Thr166 CB; Thr166 CG2; Phe103 CE1; Phe103 CE2; Phe103 CZ; Asp167 N;	7
C20	Thr166 CB; Phe103 CE2; Asp167 N; Asp167 CA; Lys48 CD; Lys48 NZ;	6
O21	Lys48 CE; Lys48 NZ;	2
C22	Glu153 O; Asn154 OD1;	2
C24	Glu153 O; Glu153 C; Glu153 CB; Asn154 OD1;	4
C26	Arg27 O;	1
C27	Arg27 C; Arg27 O;	2
Cl28	Glu153 CB; Lys151 CE; Lys151 NZ	3
Total		**60**
GB-P2-4'a atom	**PhKγtrnc atom**	**Number of contacts**
C1	Leu25 O;	1
C2	Glu110 CG; Leu25 O; Glu110 OE2	3
C3	Glu110 CG; Leu25 O;	2
C4	Gly109 CA; Leu25 O;	2
C5	Leu25CB;	1
C6	Leu156 CD1; Leu25 CB;	2
C9	Val33 CG2;	1
C10	Val33 CG2;	1
C11	Val33 CG2;	1
C12	Val33 CG2;	1
C13	Thr166 CB; Thr166 OG1	2
C14	Thr166 CB; Asp 167N;	2
C16	Lys48 CE; Lys48 NZ;	2
C17	Leu156 CD1; Thr166 CB; Thr166 CG2	3
O8	Leu156 CD1;	1
O15	Asp167 CB; Asp167 CA; Lys48 CD; Lys48 CE;	4
C18	Ile87 CG1; Phe103 CG; Phe103 CD2; Thr166 CB; Thr166 CG2; Phe103 CE2	6
C19	Ile87 CG2; Phe103 CG; Phe103 CD1; Phe103 CD2; Thr166 CB; Thr166 CG2; Phe103 CE1; Phe103 CE2; Phe103 CZ	9
C20	Thr166 CB; Phe103 CZ; Asp167 N;	3
O21	Lys48 CE; Lys48NZ; Asp167 CG;	3

Table 3 (*continued*)

B. Van der Waals interactions

GB-P2-4a atom	PhKγtrnc atom	Number of contacts
C22	Arg27 C; Arg27 O;	2
C24	Arg27 O;	1
C26	Glu153 O; Glu153 C; Glu153 CB; Asn154 OD1	4
C27	Glu153 O; Asn154 OD1	2
C28	Glu153 CB; Lys151 CE; Lys151 NZ;	3
O29	Lys151 CE; Lys151 NZ;	2
Total		**64**
GB-P2-4a atom	**PHKG2A atom**	**Number of contacts**
C1	Ile30 O;	1
C2	Ile30 O;	1
C3	Ile30 O; Ile30 CD1;	2
C4	Gly113 CA; Ile30 O;	2
C5	Ile30 O;	1
C6	Glu114 CD; Glu114 CG; Glu114 OE2; Ile30 O;	4
C9	Asp171 OD1; Val38 CG2;	2
C10	Glu114 OE2; Gly31 CA;	2
C12	Asp171 OD1; Val38 CG2; Asp171 OD2;	3
C13	Asp171 OD1;	1
C14	Lys53 CD; Asp171 OD1;	2
O15	Asp171 CG; Lys53 CE; Lys53 CD; Asp171 OD1; Asp171 OD2;	5
C16	Asp171 CG; Lys53 NZ; Asp171 OD1; Val38 CG2; Asp171 OD2;	5
C17	Leu160 CD1;	1
C18	Leu160 CD1;	1
C19	Phe107 CZ; Phe107 CD2; Phe107 CE2; Phe107 CG;	4
C20	Lys53 CD; Asp171 OD1; Phe107 CE2;	3
O21	Asp171 CG; Asp 171 OD1; Lys53 CE; Lys53 NZ; Asp171 OD2;	5
C22	Glu157 O; Asp171 OD2; Glu114 OE2;	3
C23	Asp171 OD2;	1
C24	Glu157 C; Glu157 CB; Asn158 OD1; Glu157 O; Asp171 OD2; Glu114 OE2	6
C25	Asn158 OD1; Asp171 OD2;	2
C26	Asp171 OD2;	1
C27	Asp171 OD2;	1
Cl28	Lys155 NZ; Lys155 CE; Glu157 CB; Asn158 OD1;	4
O29	Lys155 CE; Lys155 NZ;	2
Total		**65**
GB-P2-4'a atom	**PHKG2A atom**	**Number of contacts**
C1	Ile30 O;	1
C2	Ile30 O;	1
C3	Ile30 O; Ile30 CD1;	2
C4	Gly113 CA; Ile30 O;	2
C5	Ile30 O;	1
C6	Glu114 CD; Glu114 CG; Glu114 OE2; Ile30 O;	4
C9	Asp171 OD2, Val38 CG2;	2
C10	Glu114 OE2; Gly31 CA;	2
C12	Asp171 OD1; Val38 CG2; Asp171 OD2;	3
C13	Asp171 OD1;	1
C14	Lys53 CD; Asp171 OD1;	2
C16	Asp171 CG; Lys53 NZ; Asp171 CG; Val38 CG2; Asp171 OD2;	5
C17	Leu160 CD1;	1
C18	Leu160 CD1;	1
C19	Phe107 CZ; Phe107 CD2; Phe107 CE2; Phe107 CG;	4
C20	Lys53 CD; Asp171 OD1; Phe107 CE2;	3
C22	Glu157 O; Asp171 OD2; Glu114 OE2;	3
C23	Asp171 OD2;	1
C24	Glu157 C; Glu157 CB; Asn158 OD1; Glu157 O; Asp171 OD2; Glu114 OE2;	6
C25	Asn158 OD1; Asp171 OD2;	2
C26	Asp171 OD2;	1

(*continued on next page*)

Table 3 (*continued*)

B. Van der Waals interactions		
GB-P2-4a atom	PhKγtrnc atom	Number of contacts
C27	Asp171 OD2;	1
C28	Lys155 CE; Lys155 NZ; Glu157 CB; Asn158 OD1;	4
O15	Asp171 CG; Lys53 CE; Lys53 CD; Asp171 OD1; Asp171 OD2;	5
O21	Asp171 CG; Lys53 CE; Asp171 OD1; Asp171 OD2;	4
O29	Lys155 CE;	1
Total		**63**

stabilize via interactions with Lys53, Lys155, Asp171 this less active conformation.

3.4. Comparison with other ligands

The architecture of the ATP binding site of PhK has been previously described (Lowe et al., 1997; Johnson et al., 1998; Owen et al., 1995) and structural determinants for ATP recognition have been identified. Ligand binding studies (Begum et al., 2015; Hayes et al., 2011) on staurosporine and indirubin scaffolds revealed staurosporine (K_i = 0.37 nM), its analogue KT5720 (K_i = 18.4 nM) and indirubin 3′oxime (IC_{50} = 144 nM) as the most potent inhibitors of PhKγtrnc. All inhibitors upon binding, exploit hydrogen bond interaction mimicking the ATP's adenine hydrogen bonding to hinge region's residues Asp104 and Met106. In addition, they form direct and/or one water bridged hydrogen-bond interactions with Glu110 and Glu153 (Fig. 4). Despite the increased promiscuity of staurosporine towards kinases, its scaffold cannot be overlooked in drug design as KT5720 is a selective (Davies et al., 2000) inhibitor for PhK. Its selectivity can be partly attributed (Hayes et al., 2011) to the formation of additional water bridged contacts with the Arg27 backbone but also the non-conserved Thr166. Similarly, in the binary complex of PHKG2A with sunitinib (IC_{50} = 8.5 nM (Amemiya et al., 2015)), the inhibitor exploits the formation of hydrogen bonds with the homologous in PHKG2A, Asp108 and Met110 in addition to the formation of hydrogen bonds with Ile30 and water bridged to Asp117. The moderate potency of GB-P2-4a and GB-P2-4′a compared to staurosporine or indirubin analogues can be explained by the lack of strong hydrogen bond interactions. In fact, no hydrogen bonds with PhK's hinge region residues are predicted. In both cases, the inhibitors target a new region of the ATP site (Fig. 5) where the interaction of coumarin moiety with a conserved lysine is the dominant one.

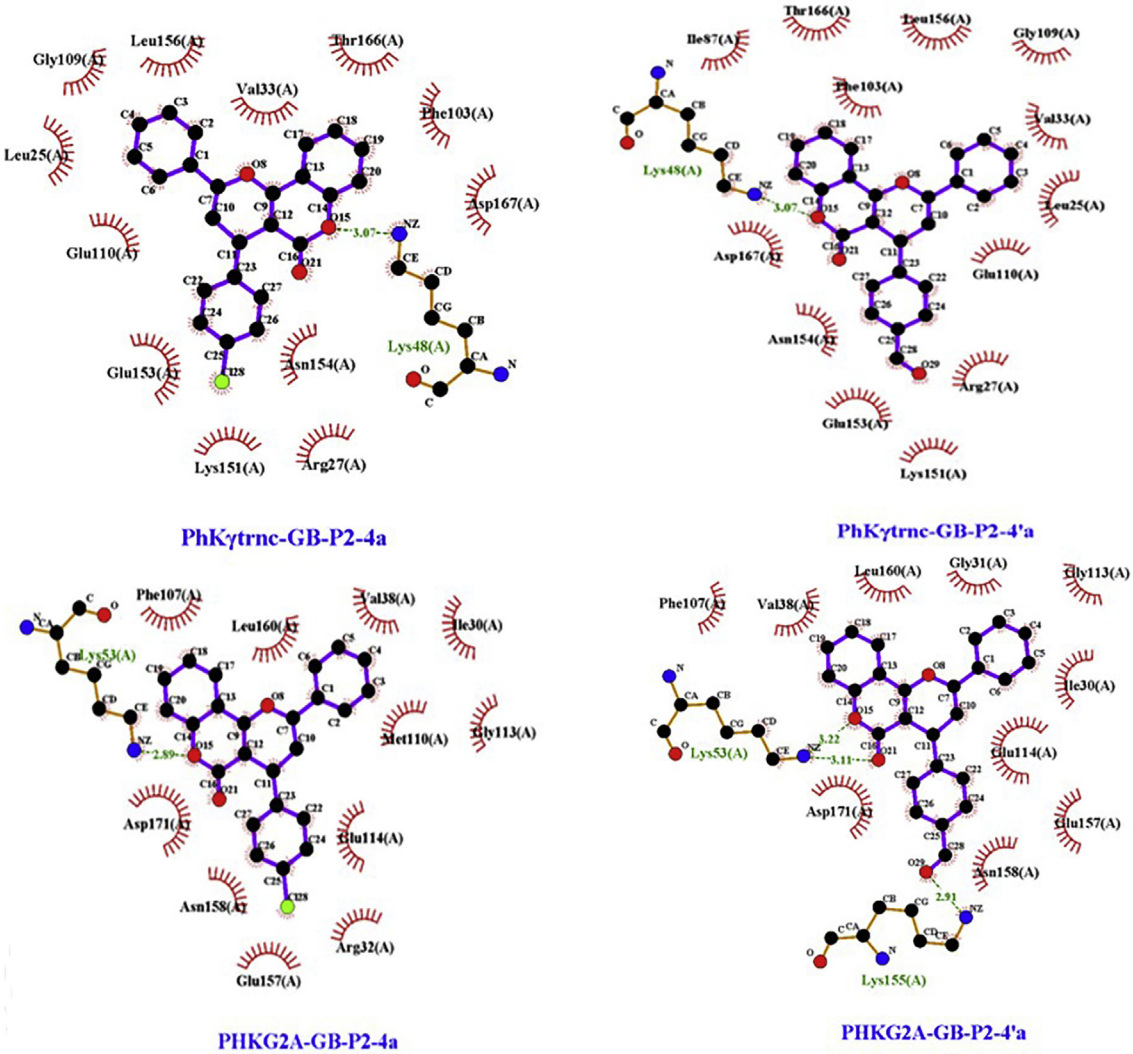

Fig. 3. LigPlot diagrams of interactions between PhK isoforms and GB-P2-4a and GB-P2-4′a. Dashed lines indicate hydrogen bonds. Halogen bonds are not depicted.

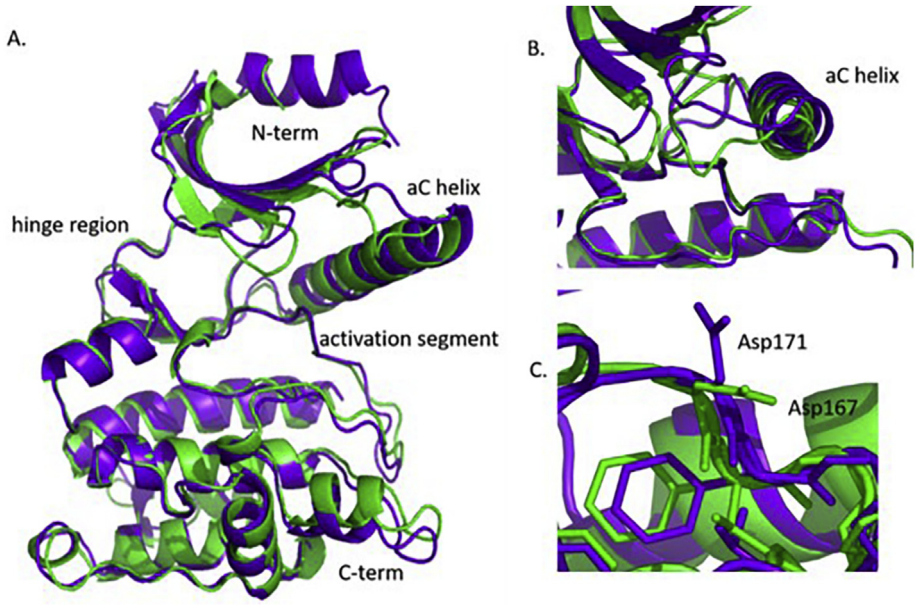

Fig. 4. A. Superposition of PhKγtrnc (green) with PHKG2A (purple). B. In case of PHKG2A complexes (purple) the aC helix adopts a "more outward" conformation. C. In PHKG2A-GB-P2-4′a complex (purple) the Asp171 is shifted with the Phe172 in the same direction seemingly adopting a "DFG out" conformation compared to the "DFG in" one for Asp167 in PhKγtrnc (green).

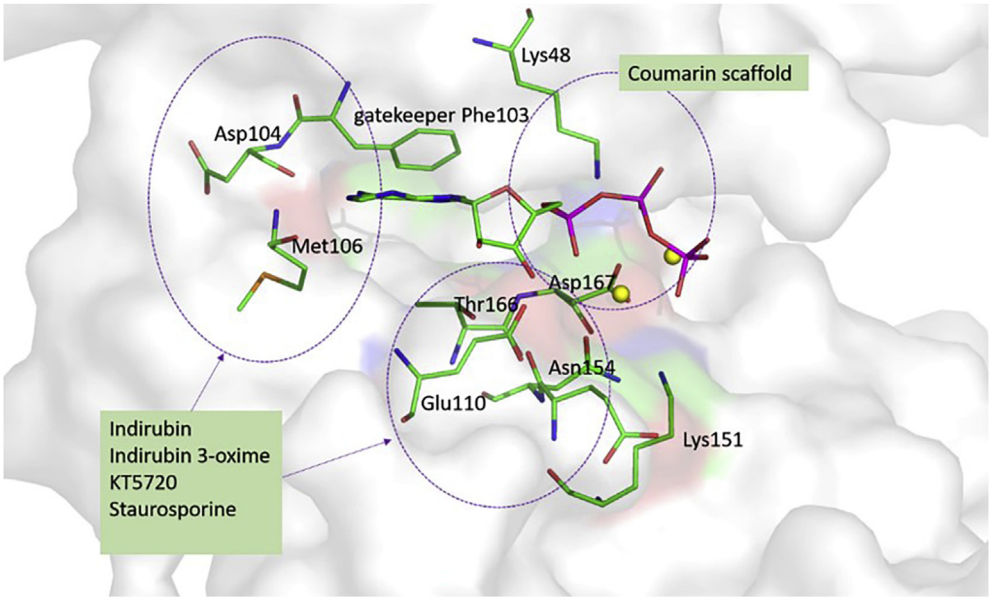

Fig. 5. Schematic representation of the regions of the ATP binding site that are targeted by the known PhK inhibitors as depicted in the PhKγtrnc-ATP/Mg2+ complex (PDB 1PhK). Coumarins target in a different area surrounding the β3-Lys (Lys48).

3.5. Implications for drug design-elements of potency and selectivity

Our study showed that GB-P2-4a and GB-P2-4′a are moderate inhibitors of PhK but in terms of rational drug design some interesting aspects were signified. The amino acid residues that decorate the ATP binding site with atoms in position to participate in interaction with inhibitors are shown in Fig. 5. The exploitation of the coumarin scaffold to target residues of the PHKG2A such as the hinge region's Asp108, Met110, Glu114, but also Glu157, Asn158, Ser, 170, Asp171, Lys53, Ile30, Arg32 (Glu153, Asn154, Thr166, Asp167, Lys48, Leu25, Arg27, in PhKγtrnc) that can participate in hydrogen bonds could improve potency. Phe107 and Phe174 (Phe103, Phe170 in PhKγtrnc) can also be exploited in hydrophobic interactions with aromatic groups of inhibitors. Amino acid sequence alignment of 50 protein kinases using the Blastp suite (Fig. 6) revealed that most residues of the ATP site are highly conserved but 4 of them, the gatekeeper Phe107, Phe174, Ser170, Arg32 (Phe103, Phe170, Thr166, Arg27 in PhKγtrnc) are not conserved, 3 of which (Phe107, Ser170, Arg32) interact with atoms of GB-P2-4a and GB-P2-4′a (Table 3B) providing elements of selectivity. In conclusion, for the pharmacological target of PHKG2A our study revealed that the coumarin analogues GB-P2-4a and GB-P2-4′a target a new region of the ATP site of the PhK (different from the usual adenine's binding site) exploiting numerous van der Waals interactions and hydrogen bonding between their coumarin moiety with a conserved Lys53. Additional interactions of both inhibitors with Lys155 and Asp171 stabilize PhK in a less active kinase conformation. This region

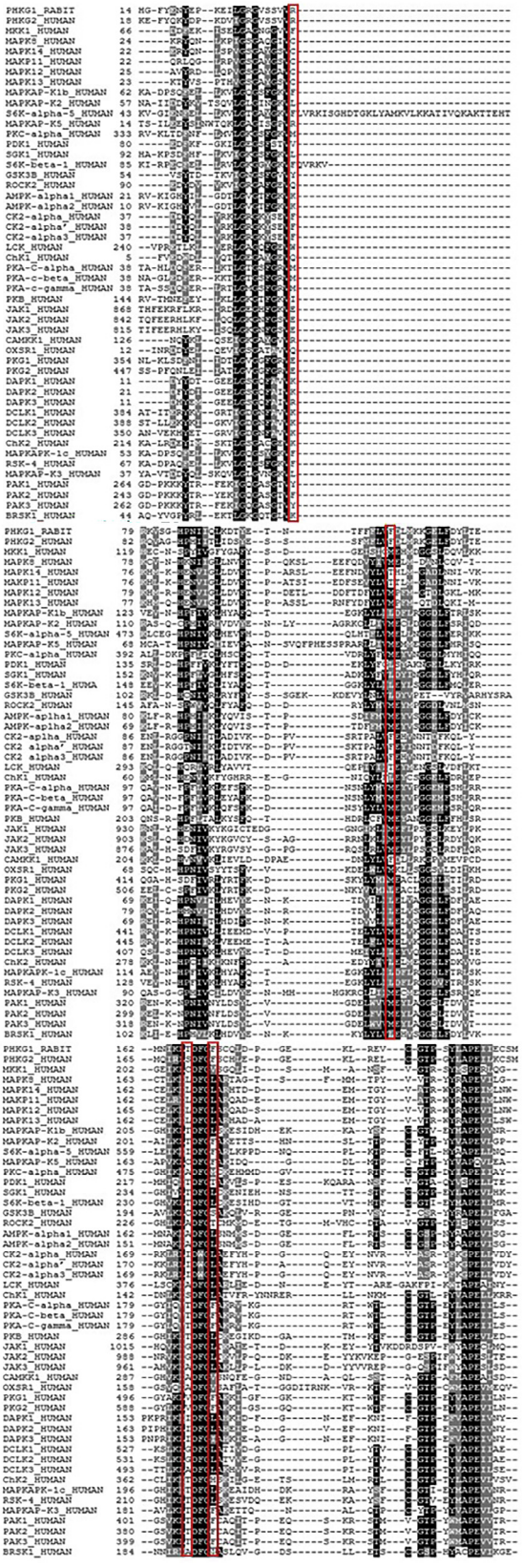

Fig. 6. Multiple sequence alignment of the kinase domain of 50 protein kinases by T-coffee (Notredame et al., 2000) The non-conserved amino acids (Arg 27, Phe 103, Thr166, Phe 170 in PhKγtrnc) of the ATP binding site are shown in the red boxes. This figure was prepared using Boxshade bio tool.

includes most of the non-conserved residues in PhK that their interactions with ATP competitive inhibitors could be exploited to confer selectivity.

Declaration of competing interest

The authors declare that they have no known competing financial interests or personal relationships that could have appeared to influence the work reported in this paper.

Acknowledgements

This work was implemented under the Postgraduate Studies Program "Biotechnology-Quality Assessment in Nutrition and Environment" Department of Biochemistry and Biotechnology, University of Thessaly. We acknowledge support of this work by the project "The National Research Infrastructures on integrated biology, drug screening efforts and drug target functional characterization – INSPIRED-Thessaly" (MIS 5002550) which is implemented under the Action "Reinforcement of the Research and Innovation Infrastructure", funded by the Operational Program "Competitiveness, Entrepreneurship and Innovation" (NSRF 2014–2020) and co-financed by Greece and the European Union (European Regional Development Fund).

References

Adasme, M.F., Linnemann, K.L., Bolz, S.N., Kaiser, F., Salentin, S., Haupt, V.J., Schroeder, M., 2021. Plip 2021: expanding the scope of the protein-ligand interaction profiler to DNA and RNA. Nucleic Acids Res. 49, W530–W534.

Aiston, S., Coghlan, M.P., Agius, L., 2003. Inactivation of phosphorylase is a major component of the mechanism by which insulin stimulates hepatic glycogen synthesis. Eur. J. Biochem. 270, 2773–2781.

Amemiya, T., Honma, M., Kariya, Y., Ghosh, S., Kitano, H., Kurachi, Y., Fujita, K.I., Sasaki, Y., Homma, Y., Abernethy, D.R., Kume, H., Suzuki, H., 2015. Elucidation of the molecular mechanisms underlying adverse reactions associated with a kinase inhibitor using systems toxicology. NPJ Syst. Biol. Appl. 1, 15005.

Begum, J., Skamnaki, V.T., Moffatt, C., Bischler, N., Sarrou, J., Skaltsounis, A.L., Leonidas, D.D., Oikonomakos, N.G., Hayes, J.M., 2015. An evaluation of indirubin analogues as phosphorylase kinase inhibitors. J. Mol. Graph. Model. 61, 231–242.

Bradford, M.M., 1976. A rapid and sensitive method for the quantitation of microgram quantities of protein utilizing the principle of protein-dye binding. Anal. Biochem. 72, 248–254.

Brahmachari, G., Nurjamal, K., 2017. Facile and chemically sustainable catalyst-free synthesis of diverse 2-Aryl-4-Alkyl/Aryl-Pyrano[3,2-c]chromen-5 (4H)-Ones by one-pot multicomponent reactions at room temperature. ChemistrySelect 2, 3695–3702.

Camus, S., Quevedo, C., Menendez, S., Paramonov, I., Stouten, P.F., Janssen, R.A., Rueb, S., He, S., Snaar-Jagalska, B.E., Laricchia-Robbio, L., Izpisua Belmonte, J.C., 2012. Identification of phosphorylase kinase as a novel therapeutic target through high-throughput screening for anti-angiogenesis compounds in zebrafish. Oncogene 31, 4333–4342.

Davies, S.P., Reddy, H., Caivano, M., Cohen, P., 2000. Specificity and mechanism of action of some commonly used protein kinase inhibitors. Biochem. J. 351, 95–105.

DeLano, W.L., 2002. The PyMOL Molecular Graphics System. DeLano Scientific, Palo Alto, CA, USA.

Drakou, C.E., Gardeli, C., Tsialtas, I., Alexopoulos, S., Mallouchos, A., Koulas, S.M., Tsagkarakou, A.S., Asimakopoulos, D., Leonidas, D.D., Psarra, A.G., Skamnaki, V.T., 2020. Affinity crystallography reveals binding of pomegranate juice anthocyanins at the inhibitor site of glycogen phosphorylase: the contribution of a sugar moiety to potency and its implications to the binding mode. J. Agric. Food Chem. 68, 10191–10199.

Harder, E., Damm, W., Maple, J., Wu, C., Reboul, M., Xiang, J.Y., Wang, L., Lupyan, D., Dahlgren, M.K., Knight, J.L., Kaus, J.W., Cerutti, D.S., Krilov, G., Jorgensen, W.L., Abel, R., Friesner, R.A., 2016. OPLS3: a force field providing broad coverage of drug-like small molecules and proteins. J. Chem. Theor. Comput. 12, 281–296.

Hayes, J.M., Skamnaki, V.T., Archontis, G., Lamprakis, C., Sarrou, J., Bischler, N., Skaltsounis, A.L., Zographos, S.E., Oikonomakos, N.G., 2011. Kinetics, in silico docking, molecular dynamics, and MM-GBSA binding studies on prototype indirubins, KT5720, and staurosporine as phosphorylase kinase ATP-binding site inhibitors: the role of water molecules examined. Proteins 79, 703–719.

Johnson, L.N., 2009a. The regulation of protein phosphorylation. Biochem. Soc. Trans. 37, 627–641.

Johnson, L.N., 2009b. Protein kinase inhibitors: contributions from structure to clinical compounds. Q. Rev. Biophys. 42, 1–40.

Johnson, L.N., Lowe, E.D., Noble, M.E., Owen, D.J., 1998. The Eleventh Datta Lecture. The structural basis for substrate recognition and control by protein kinases. FEBS Lett. 430, 1–11.

Katsori, A.M., Hadjipavlou-Litina, D., 2014. Coumarin derivatives: an updated patent review (2012-2014). Expert Opin. Ther. Pat. 24, 1323–1347.
Kaur, M., Kohli, S., Sandhu, S., Bansal, Y., Bansal, G., 2015. Coumarin: a promising scaffold for anticancer agents. Anti Cancer Agents Med. Chem. 15, 1032–1048.
Leatherbarrow, R.J., 2007. GrafFit Version 6.0. Erithakus Software, Staines, UK.
Lowe, E.D., Noble, M.E., Skamnaki, V.T., Oikonomakos, N.G., Owen, D.J., Johnson, L.N., 1997. The crystal structure of a phosphorylase kinase peptide substrate complex: kinase substrate recognition. EMBO J. 16, 6646–6658.
Mosmann, T., 1983. Rapid colorimetric assay for cellular growth and survival: application to proliferation and cytotoxicity assays. J. Immunol. Methods 65, 55–63.
Nasr, T., Bondock, S., Youns, M., 2014. Anticancer activity of new coumarin substituted hydrazide-hydrazone derivatives. Eur. J. Med. Chem. 76, 539–548.
Notredame, C., Higgins, D.G., Heringa, J., 2000. T-Coffee: a novel method for fast and accurate multiple sequence alignment. J. Mol. Biol. 302, 205–217.
Owen, D.J., Noble, M.E., Garman, E.F., Papageorgiou, A.C., Johnson, L.N., 1995. Two structures of the catalytic domain of phosphorylase kinase: an active protein kinase complexed with substrate analogue and product. Structure 3, 467–482.
Pereira, T.M., Franco, D.P., Vitorio, F., Kummerle, A.E., 2018. Coumarin compounds in medicinal chemistry: some important examples from the last years. Curr. Top. Med. Chem. 18, 124–148.
Roskoski Jr., R., 2015. A historical overview of protein kinases and their targeted small molecule inhibitors. Pharmacol. Res. 100, 1–23.
Scapin, G., Patel, S.B., Becker, J.W., Wang, Q., Desponts, C., Waddleton, D., Skorey, K., Cromlish, W., Bayly, C., Therien, M., Gauthier, J.Y., Li, C.S., Lau, C.K., Ramachandran, C., Kennedy, B.P., Asante-Appiah, E., 2003. The structural basis for the selectivity of benzotriazole inhibitors of PTP1B. Biochemistry 42, 11451–11459.
Schrödinger, 2018. LLC. New York, NY.
Skamnaki, V.T., Oikonomakos, N.G., 2000. Kinetic characterization of the double mutant R148A/E182S of glycogen phosphorylase kinase catalytic subunit: the role of the activation loop. J. Protein Chem. 19, 499–505.
Skamnaki, V.T., Owen, D.J., Noble, M.E., Lowe, E.D., Lowe, G., Oikonomakos, N.G., Johnson, L.N., 1999. Catalytic mechanism of phosphorylase kinase probed by mutational studies. Biochemistry 38, 14718–14730.
Sondergaard, C.R., Olsson, M.H., Rostkowski, M., Jensen, J.H., 2011. Improved treatment of ligands and coupling effects in empirical calculation and rationalization of pKa values. J. Chem. Theor. Comput. 7, 2284–2295.
Thakur, A., Singla, R., Jaitak, V., 2015. Coumarins as anticancer agents: a review on synthetic strategies, mechanism of action and SAR studies. Eur. J. Med. Chem. 101, 476–495.
Vulpetti, A., Bosotti, R., 2004. Sequence and structural analysis of kinase ATP pocket residues. Farmaco 59, 759–765.
Wallace, A.C., Laskowski, R.A., Thornton, J.M., 1995. LIGPLOT: a program to generate schematic diagrams of protein-ligand interactions. Protein Eng. 8, 127–134.
Winn, M.D., Ballard, C.C., Cowtan, K.D., Dodson, E.J., Emsley, P., Evans, P.R., Keegan, R.M., Krissinel, E.B., Leslie, A.G., McCoy, A., McNicholas, S.J., Murshudov, G.N., Pannu, N.S., Potterton, E.A., Powell, H.R., Read, R.J., Vagin, A., Wilson, K.S., 2011. Overview of the CCP4 suite and current developments. Acta Crystallogr. Sect. D Biol. Crystallogr. 67, 235–242.
Zuccotto, F., Ardini, E., Casale, E., Angiolini, M., 2010. Through the "gatekeeper door": exploiting the active kinase conformation. J. Med. Chem. 53, 2681–2694.